The temporal organization of corticostriatal communications

Cole Korponay[1], Ph.D., ckorponay@mclean.harvard.edu
Elliot A Stein[2], Ph.D., estein@nih.gov
Thomas J Ross[2], Ph.D., tross@nih.gov

[1]*Basic Neuroscience Division, McLean Hospital, Belmont, MA*
[2]*Neuroimaging Research Branch, Intramural Research Program, National Institute on Drug Abuse, Baltimore, MD*

Author for correspondence: Cole Korponay
ckorponay@mclean.harvard.edu
115 Mill St.
Belmont, MA 02478
(516) 669-2371

Words in Abstract: 148
Words in Main Text: 3357
Figures: 6
Tables: 1

Funding: NIDA grant 1F32DA048580-01A1 to CK and the Intramural Research Program of the National Institute on Drug Abuse to TR and EAS

The authors report no conflicts of interest.

ABSTRACT

Cortical activation of the striatum requires temporally synchronized communications from numerous afferents. However, the systems-level temporal organization of corticostriatal circuitry remains poorly understood. Applying recent advances in temporally unwrapping "edge" functional connectivity data, we identify communities of corticostriatal node-pairs with preferentially synchronized communication patterns. Strikingly, these communities are spatially orthogonal to classic gradients of corticostriatal structural and static functional connectivity. This spatiotemporal "blending" – wherein striatal nodes connected to similar areas of cortex may nonetheless communicate with these areas at different times, and vice versa – may increase the repertoire of striatal responses to frontal input and facilitate functional integration in the temporal dimension. We provide evidence that this decoupling of spatial and temporal communication patterns may stem from spatially variable modulation of striatal responsivity to cortical input by intra-striatal connections. Findings provide a framework to investigate how different corticostriatal connections coordinate in the temporal dimension to produce complex behaviors.

INTRODUCTION

As the model of brain information processing has shifted from one of local functional subunits to distributed networks[1], interest has intensified in examining synchrony between spatially distant neural activity and how this temporal coordination contributes to complex behavioral patterns in both health and disease. To this end, there has been tremendous progress in uncovering pairs and networks of brain nodes with correlated activity[2-4] and the physical tracts that facilitate this synchrony[5, 6]. Such interactions between the frontal cortex and striatum have been afforded particular focus given their centrality in myriad adaptive functions[7, 8] and in neuropsychiatric disorders, including substance use disorder (SUD), obsessive-compulsive disorder (OCD), and attention-deficit hyperactivity disorder (ADHD)[9, 10].

At any given moment, thousands of individual connections transmit communications from the frontal cortex to the striatum. A rich neuroanatomical literature has delineated much of the structural architecture that links nodes in frontal cortex to nodes in striatum[11-13], revealing a topographic organization wherein each cortical region projects preferentially to specific areas of striatum[14]. The transmission of information from frontal cortex to striatum via these projections can be inferred from correlated fMRI BOLD signal activity (i.e., static functional connectivity, FC) between cortex-striatum node-pairs[15, 16]. Though FC is a non-directional measure, and striatal activity also indirectly influences cortical activity via cortico-basal ganglia-thalamo-cortical loops, the FC strength of cortex-striatum node-pairs is strongly correlated to the strength of their direct structural connections. Thus, a topographic map of corticostriatal FC largely mirrors that of the underlying structural connectivity map[16-18]. In

aggregate, these corresponding maps of cortex-striatum node-pairs undergird much of the current understanding of interactions between these structures. This framework has engendered an often-implicit assumption that individual cortex-striatum node-pairs are the foundational unit from which behavioral functions emerge in this circuitry.

Yet, morphological and electrophysiological features of frontostriatal circuitry dictate that cortex-striatum node-pairs operate in tandem with one another, via temporal coordination of their communications. Striatal medium spiny neurons (MSNs) have expansive dendritic trees[19] that are subject throughout to a strong inwardly rectifying potassium current that keeps them in a hyperpolarized "down state" at rest[19]. Since individual cortical neurons make only a few synapses on the dendritic tree of any individual MSN[20], even repeated excitatory input from one cortical neuron tends to be insufficient to depolarize an MSN. However, individual MSNs receive afferents from thousands of neurons throughout different areas of cortex[20], and a sufficient number of temporally synchronized communications from these inputs can facilitate depolarization and subsequent firing of action potentials[20-22]. The cortical input to MSNs also tends to be spatially distributed, such that MSNs receive appreciable convergent input from diverse cortical regions[13, 23]. Together, the spatially convergent and temporally coordinated activity of many corticostriatal connections allows the striatum to be an integrator of frontal communications from different functional streams (e.g., motor, cognitive, limbic) and thereby facilitate adaptive, complex behaviors[6]. Overall, communities of cortex-striatum node-pairs (i.e., corticostriatal connections, or 'edges' in graph theory) with synchronous patterns of communication appear to represent a crucial component of corticostriatal organization and function.

Yet, the organization and properties of temporal coordination across cortex-striatum node-pairs is poorly understood. Existing structural and functional maps of node-to-node coordination do not provide information about which corticostriatal edges propagate communications that are in sync with one another. High temporal resolution local field potential (LFP) data indicate that the striatum may be spatially differentiable into subregions that have distinct communication patterns with frontal cortex. In particular, evidence exists that oscillation coherence within different cortex-striatum node-pairs occurs at specific preferred frequencies[24], is differentially modulated by the same neurotransmitters[25], and selectively increases for node-pairs actively involved in controlling behavioral output[26]. However, despite the high temporal and spatial resolution of LFP recording techniques, these methods are limited to examining a small subset of the cortical and striatal landscape. As such, a systems-level mapping of the temporal organization of corticostriatal circuitry is lacking.

Emerging methods[27, 28] that allow for time-resolved analysis of "edge" FC interactions, and which can canvass the activity of all of frontal cortex and striatum at millimeter spatial resolution, offer a potential window into this systems-level organization. These methods exploit the finding that much of static FC coherence between two nodes appears to be driven by just a handful of discrete, high-coordination time points – moments that putatively represent bursts of communication between the nodes[29]. Unwrapping the static FC Pearson correlation coefficient between two nodes' BOLD timeseries (i.e., their *average* level of coactivation across time) can therefore yield an "edge time series" (eTS) that delineates the magnitude of the node-pair's coactivation at each point in time. This in turn allows for the computation of "edge functional connectivity" (eFC) between any two edges'

eTSs, denoting the synchrony of their coactivation patterns (and putatively, of their communication bursts)[27, 28].

Here, we adapt these methods to elucidate the temporal organization of corticostriatal communications. We first demonstrate the existence of corticostriatal node-pair communities with synchronous coactivation patterns. Strikingly, we show that the spatial organization of these communities is largely orthogonal to the classic gradients of corticostriatal structural and static functional connectivity. Further, we provide evidence that this orthogonal orientation may stem from spatially diverse modulation of striatal responsivity to cortical input by intra-striatal connections.

RESULTS

The Magnitude of Synchrony between Different Corticostriatal Communications

We performed discovery analyses on resting BOLD data from a cohort of 77 unrelated adult subjects from the Human Connectome Project (HCP) dataset[30] curated by Chen and colleagues [31] to meet stringent standards for low head-motion during scanning (see Methods for full cohort details). For each subject we computed the edge time series (eTS, quantifying the magnitude of coactivation between an edge's two nodes at each time point) for 51,300 corticostriatal edges involving the right striatum (1710 striatal voxels * 30 frontal cortical regions of interest), and for 51,360 corticostriatal edges involving the left striatum (1712 striatal voxels * 30 frontal cortical regions of interest). Frontal cortical regions of interest (ROIs) were derived from the Harvard-Oxford atlas. Subsequently, for each subject, we computed the temporal correlation between every pair of edge time series (edge functional connectivity, eFC), quantifying the magnitude of synchrony between edges' coactivation patterns (**Figure 1**). The eFC matrix of each subject was averaged together to establish a group mean eFC matrix, upon which subsequent analyses of interest were performed.

Figure 1.

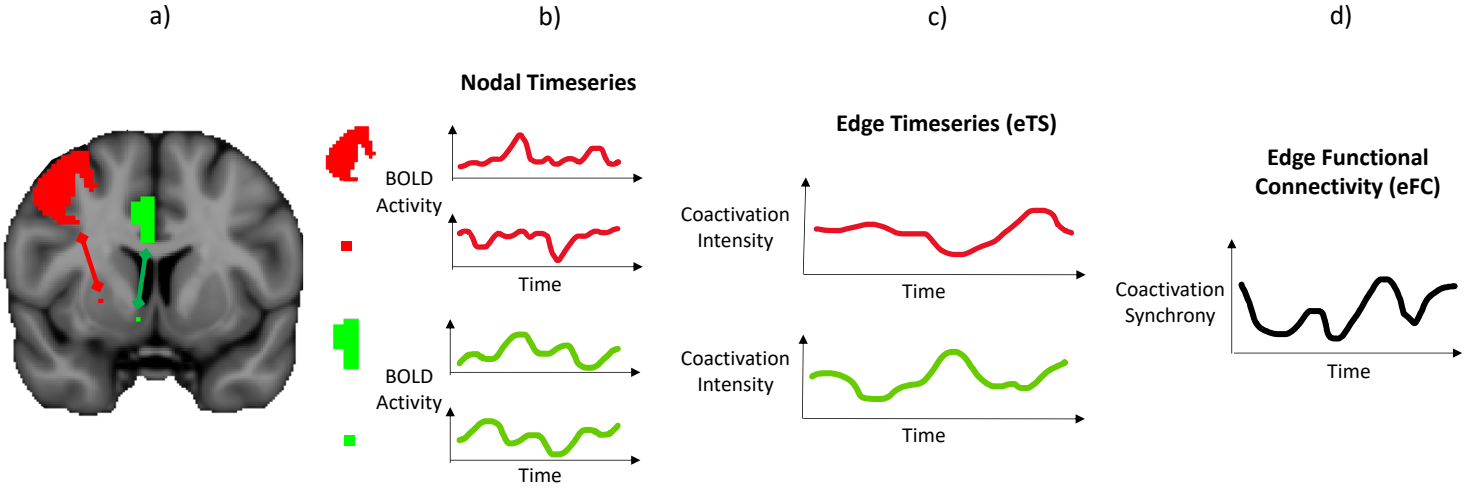

Figure 1. Overview of analysis pipeline. a) Each corticostriatal edge links one cortical node to one striatal node. b) Each node comprising the edge has a "nodal timeseries" quantifying its BOLD activation magnitude across time. c) The correspondence at each time point between the magnitudes of the two nodal timeseries comprising an edge is quantified by the "edge timeseries" (eTS), a putative measure of the communication pattern across the edge. d) Finally, the correlation between any two eTSs is quantified by edge functional connectivity (eFC). We define this as a measure of synchrony between two corticostriatal edges' communication patterns.

First, we examined the distribution of eFC values across all corticostriatal edge-pairs. We found that 94% of all 1,315,818,540 examined corticostriatal edge-pairs involving the right striatum and 95% of all 1,318,898,310 examined corticostriatal edge-pairs involving the left striatum have very low coactivation synchrony with each other (i.e., edge time series with eFC < 0.2) (**Figure 2**). The preponderance of low-synchrony edge-pairs implies an enormous diversity of node-pair communication patterns. Indeed, on average, a given corticostriatal edge was found to have an eFC > 0.9 with only 2.32 other edges (0.005% of all other edges), and an eFC > 0.5 with only 135.33 other edges (0.264% of all other edges). Overall, eFC values ranged from a low of -0.268 to a high of 0.945. To determine statistically significant eFC values, we established a null distribution of eFC values computed between 2.6 billion random pairs of across-subject eTSs, wherein each eFC value is computed from two eTSs that are statistically independent. $p<0.001$ corresponded to eFC>0.226 (**Figure S1**).

Figure 2.

a)

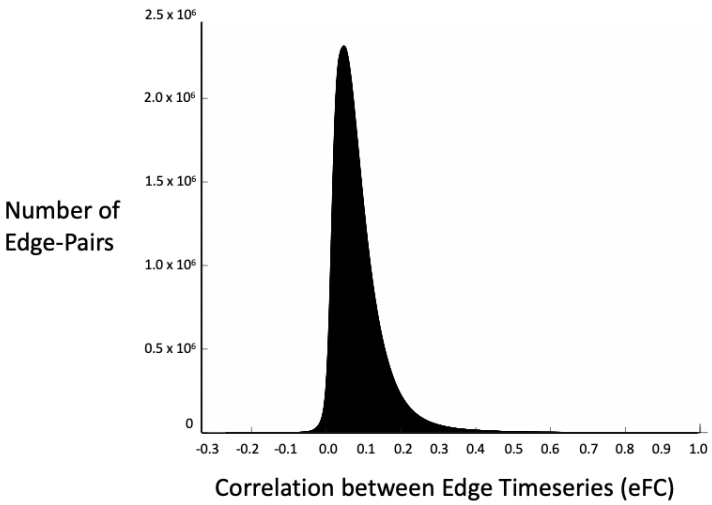

b)

eFC	Total	%
-0.3 – -0.2	4879	0.0004
-0.2 – -0.1	185029	0.0141
-0.1 – 0.0	16793628	1.2763
0.0 – 0.1	899391953	68.3523
0.1 – 0.2	322313983	24.4953
0.2 – 0.3	54816400	4.1660
0.3 – 0.4	13498358	1.0259
0.4 – 0.5	5032287	0.3824
0.5 – 0.6	2122262	0.1613
0.6 – 0.7	992058	0.0754
0.7 – 0.8	356737	0.0271
0.8 – 0.9	251463	0.0191
0.9 – 1.0	59503	0.0045

Figure 2. a) Distribution of eFC values across all pairs of corticostriatal edges (right striatum) b) For each range of eFC values, the total number of corticostriatal edge-pairs with an eFC value in that range and the percent of all corticostriatal edge-pairs that total represents.

Next, we examined eFC values amongst different corticostriatal edge-pair "types" (**Figure S2**). We defined five distinct types of corticostriatal edge-pairs. Type 1 edge-pairs are those formed by a single striatal node's connections to homotopic cortical nodes. Type 2 edge-pairs are those formed via a single striatal node's connections to non-homotopic cortical nodes. Type 3 edge-pairs are those formed via a single cortical node's connections to two spatially separated striatal nodes. Type 4 edge-pairs are those formed via two homotopic cortical node's connections to two spatially separated striatal nodes. Type 5 edge-pairs are those formed via two non-homotopic cortical nodes' connections to two spatially separated striatal nodes. Amongst these five categories of examined edge-pair types, those formed by a single striatal node's connections to homotopic cortical nodes (Type 1 edge-pairs) had by far the highest average eFC value (eFC_{avg} = 0.695, $p<0.0000001$) (**Table 1**, **Figure S3**), as might be expected

given the strong cortico-cortical connections and high level of coordination between homotopic cortical nodes. The next highest average eFC (eFC_{avg} = 0.309, p<0.0001) was amongst edges formed via a single striatal node's connections to non-homotopic cortical nodes (Type 2 edge-pairs), likely reflecting the electrophysiological requirement of striatal nodes to receive temporally aligned communications from its frontal inputs in order to fire action potentials. In contrast, the magnitude of coactivation synchrony amongst edge-pairs formed by two spatially separated striatal nodes and any combination of cortical nodes (Type 3-5 edge-pairs) was low (eFC_{avg} < 0.175, p<0.01). Such edge-pairs involving either the same cortical node (Type 3, eFC_{avg} = 0.172, p<0.01) or homotopic cortical nodes (Type 4, eFC_{avg} = 0.130, p<0.05) expectedly had coactivation synchrony magnitudes approximately twice as high as those involving two non-homotopic cortical nodes (Type 5, eFC_{avg} = 0.073, p>0.1), whose eTSs were mostly unrelated to each other (**Table 1**, **Figure S3**).

Table 1.

Edge-Pair Types

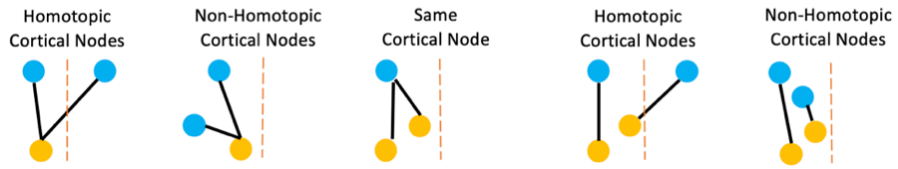

Number of Edge-Pairs in Coactivation Synchrony Range					
-0.3 ≤ eFC < -0.2	0	1676	0	0	135
-0.2 ≤ eFC < -0.1	0	6411	0	0	17332
-0.1 ≤ eFC < 0.0	0	16390	1957	3586	8273959
0.0 ≤ eFC < 0.1	0	86298	4479457	9378332	**532055833**
0.1 ≤ eFC < 0.2	0	**131065**	**13074300**	**12240534**	145272004
0.2 ≤ eFC < 0.3	0	129108	5787553	2760382	11882810
0.3 ≤ eFC < 0.4	1660	122351	1119802	426444	1583403
0.4 ≤ eFC < 0.5	2237	98727	307217	112182	366713
0.5 ≤ eFC < 0.6	3791	51993	111091	41544	85756
0.6 ≤ eFC < 0.7	5576	47246	66083	12326	18355
0.7 ≤ eFC < 0.8	3771	26913	20448	4810	506
0.8 ≤ eFC < 0.9	**8614**	22	12884	355	0
0.9 ≤ eFC ≤ 1.0	4	0	3252	0	0
Mean eFC	0.695	0.309	0.172	0.130	0.073

Table 1. Number of edge-pairs involving right striatum in each eFC range by edge-pair type. Bolding indicates each edge-pair type's most common eFC range. Bottom row presents the mean eFC of each edge-pair type.

We corroborated the distribution of these observed corticostriatal eFC properties in an independent matched replication sample (n=77) and demonstrated nearly identical correspondence between the eFC matrices of the discovery and replication samples in both the right striatum ($r = 0.975$, $p<0.0001$) and left striatum ($r = 0.973$, $p<0.0001$) (**Figure S4**). These findings indicate that this temporal organization is highly consistent and reproducible across individuals.

Coactivation Synchrony Communities: Corticostriatal Connections with Similar Communication Patterns

Next, we sought to identify communities of cortex-striatum node pairs with similar patterns of coactivation across time, as a putative measure of which corticostriatal connections have synchronized communication patterns. To do so, we performed k-means clustering on the group eFC matrix. At all values of k=2 through k=10, k-means clustering identified communities of cortex-striatum node-pairs whose coactivation patterns were significantly ($p <0.0001$) more synchronized with each other than with node-pairs outside the community. For instance, at k=6, the average eFC between edges within communities was 0.448, 0.410, 0.211, 0.598, 0.458, and 0.501 for Community 1 through Community 6, respectively. Contrarily, the average eFC with edges outside of the community was 0.095, 0.081, -0.047, 0.059, 0.066, and 0.185 for Community 1 through Community 6, respectively. Examination of edge time series at the subject level illustrates the unique temporal coactivation pattern of each community (**Figure 3**),

where the average edge time series of each community has a distinct pattern of coactivation magnitude across time.

Figure 3.

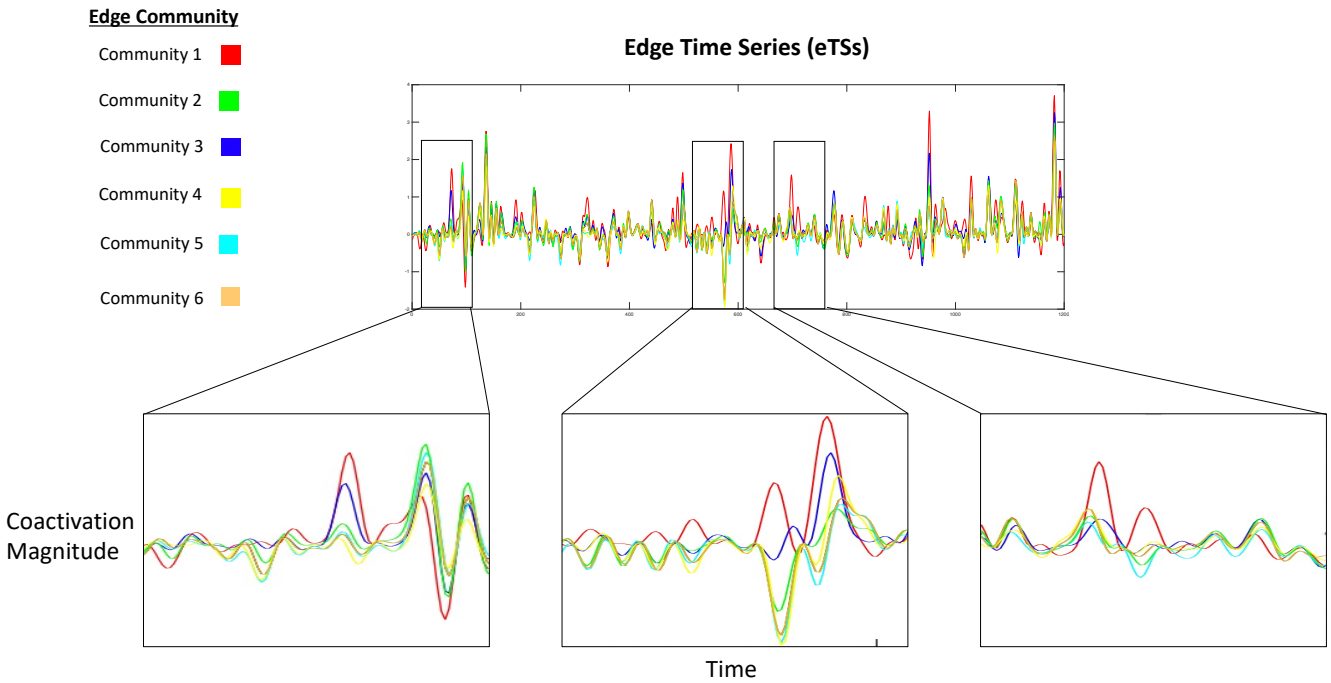

Figure 3. The average edge timeseries (eTS) of edges belonging to each of k=6 coactivation synchrony communities for a representative subject. Edges in each community have a distinct pattern of coactivation magnitude across time.

Each striatal node participates in 30 edges (i.e., one with each of the 30 frontal cortical nodes), and each of these edges belongs to one of *k* coactivation synchrony communities (as determined from the k-means clustering analysis). Thus, each striatal voxel has a multivariate profile of coactivation synchrony community membership (**Figure S5**). In order to facilitate spatial visualization of where corticostriatal connections with similar communication patterns are located, we assigned each striatal voxel to its strongest (i.e., modal) coactivation synchrony community. **Figure 4** illustrates the spatial organization of striatal voxels assigned to their

modal coactivation synchrony community, for k=2 through k=10. We found that the number of different strongest communities assigned to striatal voxels reached a maximum at k=6.

Figure 4.

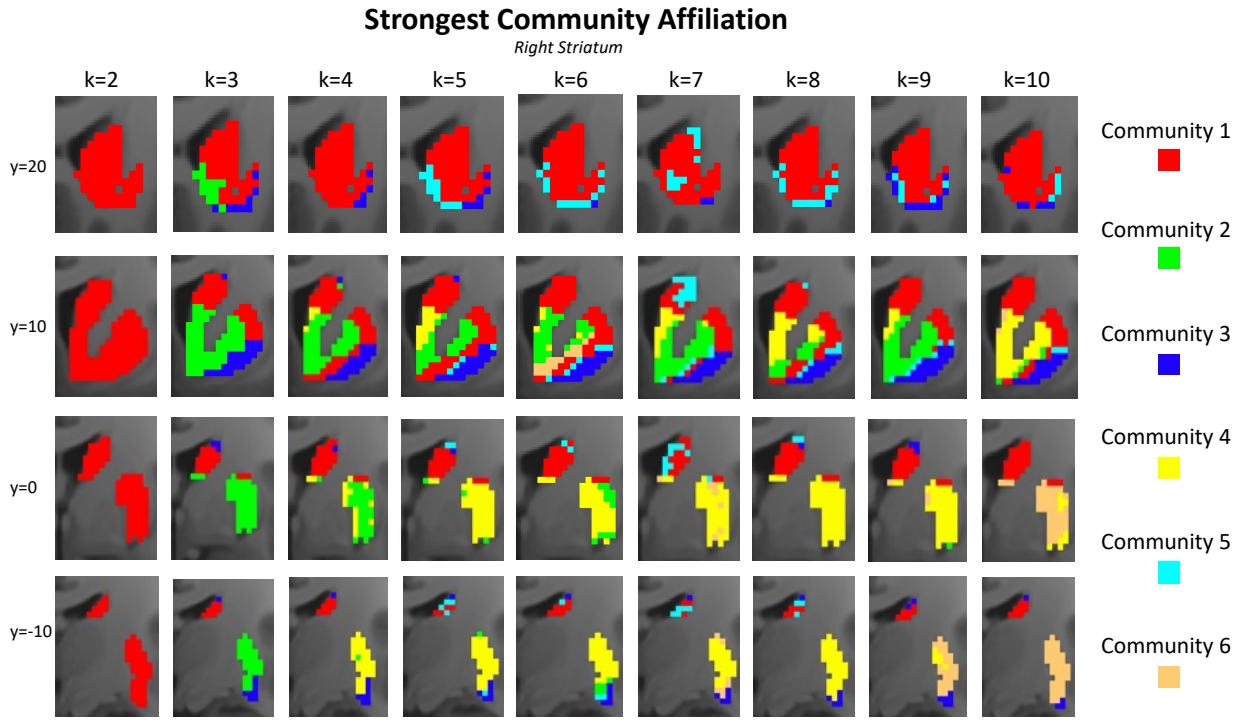

Figure 4. For each integer value of *k*=2 through *k*=10, the modal coactivation synchrony community of each striatal voxel, determined from the community assignments of each voxel's 30 edges. The number of distinct modal communities reached a maximum of 6 even when *k* exceeded 6.

Common across all clustering solutions of k=3 through k=10 was 1) a community (*red*) that occupied the rostral striatal pole, dorsal caudate and dorsal putamen, and a narrow strip from the lateral ventral striatum to the dorsal putamen spanning the medial putamen; 2) a community (*green*) that occupied the central striatum including the ventral caudate, ventromedial putamen, and nucleus accumbens; and 3) a community (*dark blue*) that occupied

the ventral lateral putamen. A maximum of three additional communities (4-6) emerged in differing locations at higher levels of *k*.

Corticostriatal Coactivation Synchrony Communities are Orthogonal to Corticostriatal Functional Connectivity Communities

The above results illustrate that, regardless of *k*, the spatial map of coactivation synchrony communities in the striatum is oriented in a ventromedial-to-dorsolateral fashion. Strikingly, this spatial structure is seemingly orthogonal to the dorsomedial-to-ventrolateral spatial parcellation that emerges from classic maps of frontostriatal structural[6] and functional connectivity (**Figure 5**).

Figure 5.

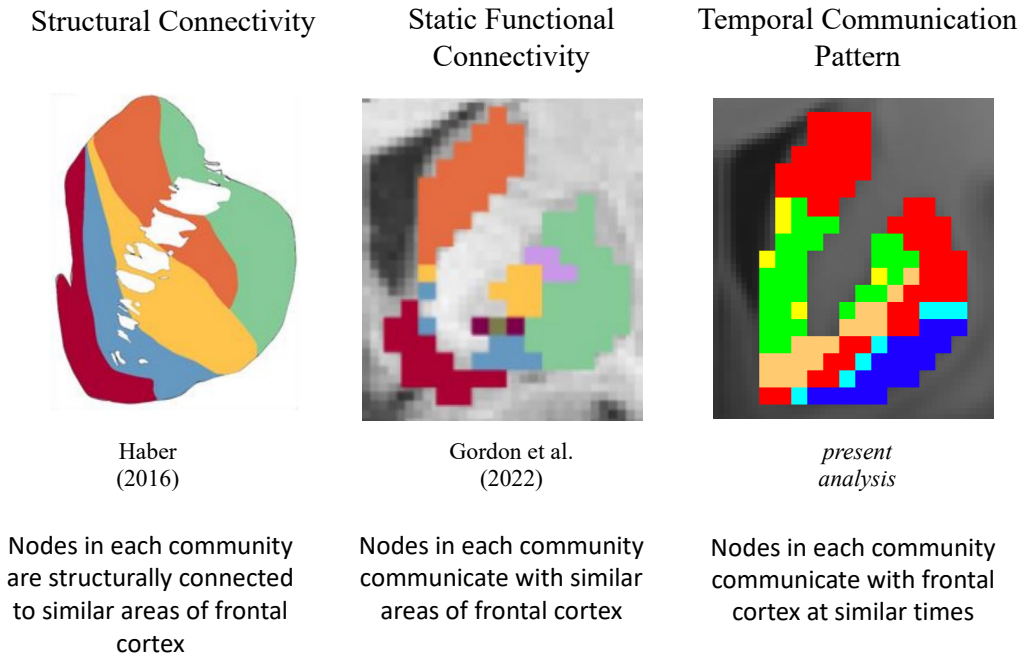

Figure 5. The mismatch between parcels of striatal space with similar frontal cortical structural and static functional connectivity and parcels with similar frontal cortical temporal communication patterns, illustrating "spatiotemporal blending". Images in the left and middle panels are adapted from Haber (2016)[6] and Gordon et al. (2022)[17], respectively.

These data suggest that two striatal nodes with similar frontal cortical connectivity profiles – receiving similarly timed communications from similar inputs – may nonetheless have different temporal patterns of frontal coactivation. Conversely, two striatal nodes with dissimilar frontal cortical connectivity profiles may nonetheless have similar temporal patterns of frontal coactivation.

Variance in Modulatory Input Profiles as a Candidate Mechanism for Decoupling Corticostriatal Static Connectivity from Corticostriatal Temporal Dynamics

We next explored what might allow two striatal nodes with similar frontal cortical static FC profiles to nonetheless have different patterns of frontal cortical coactivation. In addition to frontal input, striatal nodes receive substantial input from other areas of the striatum, the dopaminergic midbrain, and the thalamus. Moreover, these inputs have been found to modulate, or "gate", the responsivity of striatal nodes to frontal cortical input[32-36]. Thus, theoretically, two striatal nodes connected to similar frontal cortical areas could have diverse coactivation patterns with these areas if the nodes have different profiles of modulatory connectivity that differentially gate their responsivity to cortical input. For this to be a viable mechanism, we should expect the spatial organization of striatal communities with similar frontal cortical FC profiles to be *distinct* from the spatial organization of striatal communities with similar intra-striatal, midbrain, and/or thalamic FC profiles. Furthermore, if one or more of

these modulatory inputs indeed shape corticostriatal temporal coactivation patterns, then we should expect to observe *alignment* between the spatial organization of striatal communities with similar modulatory input FC profiles and similar frontal coactivation patterns.

To investigate this model, we compared the spatial distribution of striatal nodes with similar intra-striatal (**Figure 6a**), midbrain (**Figure 6b**), and thalamic (**Figure 6c**) static FC profiles to the spatial distribution of striatal nodes with similar frontal cortical static FC profiles (**Figure 6d**) and to the spatial distribution of striatal nodes with similar frontal cortical coactivation patterns (**Figure 6e**, as computed in the previous analysis (**Figure 3**)). We computed the spatial correlation (Pearson's *R*) between these maps as a measure of alignment. Of the three modulatory inputs, the spatial organization of intra-striatal connections fit the hypothesized model most strongly (**Figure 6a**), displaying weak alignment with frontal FC profiles (R=0.238 and R=0.356 for k=3 and k=6, respectively) and strong alignment with frontal coactivation patterns (R=0.864 and R=0.652 for k=3 and k=6, respectively). Midbrain-striatal connections also displayed weak alignment with frontal FC profiles and moderate alignment with frontal coactivation patterns (**Figure 6b**). Thalamic-striatal connections displayed weak alignment with both frontal FC profiles and frontal coactivation patterns (**Figure 6c**).

Figure 6.

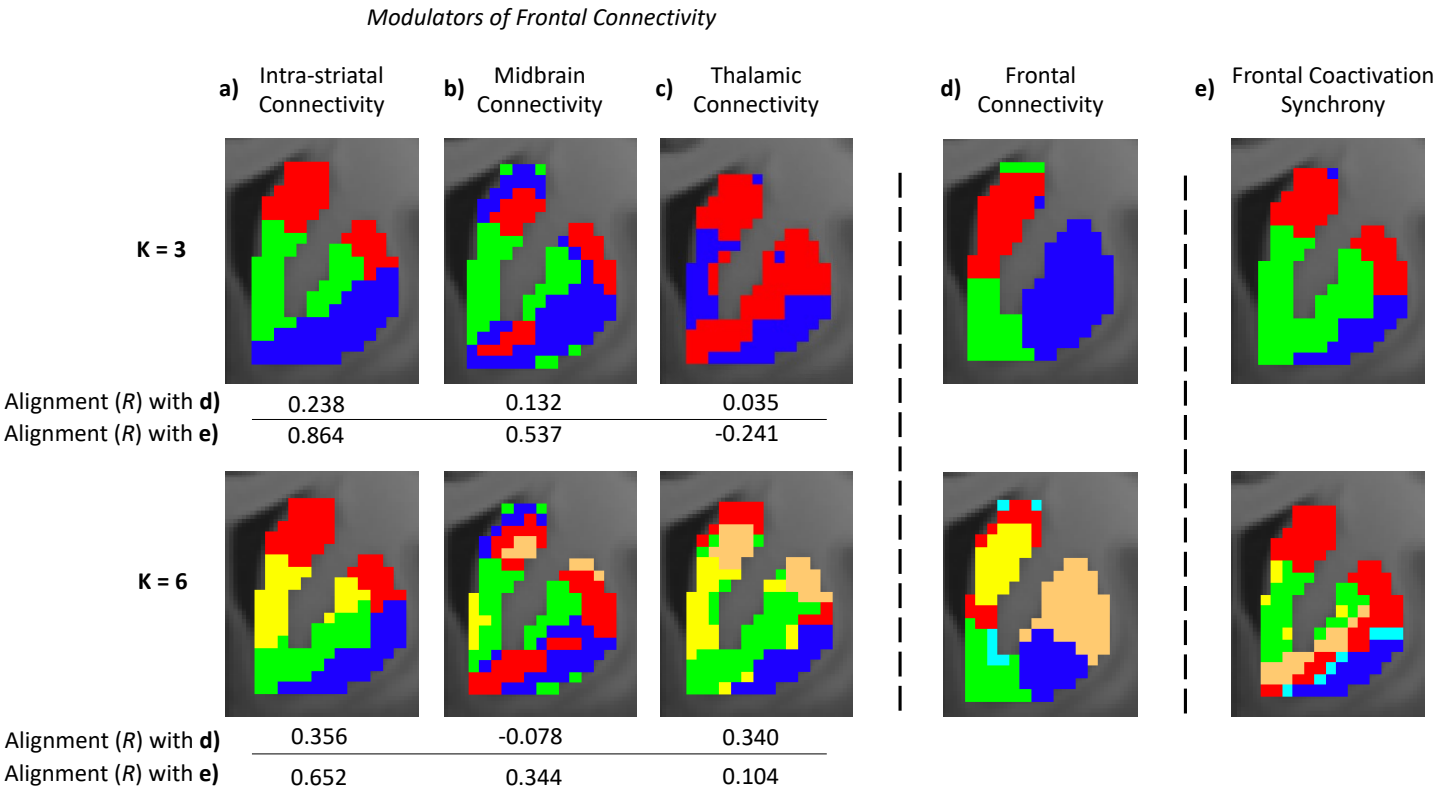

Figure 6. Visualizing the quantitative alignment between striatal communities with similar a) intra-striatal, b) midbrain-striatal, and c) thalamo-striatal static FC profiles and striatal communities with similar d) fronto-striatal static FC profiles and e) fronto-striatal temporal communication patterns.

Collectively, these data suggest that two striatal nodes with similar frontal cortical connectivity profiles – receiving similarly timed communications from similar frontal inputs – may nonetheless have different frontal coactivation patterns if they have different modulatory intra-striatal and/or midbrain input profiles. At any given moment in time, these modulatory inputs may differentially gate the responsivity of the striatal nodes to their cortical inputs.

Synchrony and Entropy within Striatal Coactivation Profiles

Lastly, we investigated spatial variance in the coherence and diversity of each striatal voxel's set of frontal cortical edges. We defined "synchrony" as the average eFC amongst all paired combinations of a given striatal voxel's 30 frontostriatal edge time series. This measure provides a putative gauge of how aligned a striatal node's frontal cortical communications are. We found that the bilateral ventromedial striatum, bilateral dorsolateral caudate, and left lateral caudate displayed disproportionately more synchrony amongst their frontal cortical communications than the rest of the striatum (using the interquartile range (IQR) criterion for outlier detection[37]) (**Figure S6**).

We also computed the "entropy"[38] of each striatal voxel's edge community profile as a putative measure of the diversity of its frontal cortical communication patterns. **Figure S7** illustrates voxel-wise entropy values throughout the striatum for *k*=2 through *k*=10. Common across all clustering solutions, entropy reaches a minimum in a defined area of the ventral lateral putamen and a maximum in areas of the rostral ventral striatum.

DISCUSSION

The Hebbian principle holds that brain nodes that are active at the same time are likely involved in a common functional process[39]. In an edge-centric interpretation of this principle, connections that transmit communications at the same time are also likely involved in a common functional process. This notion comes to bear concretely in the striatum, where individual MSNs must receive temporally aligned communications from many of their afferents as a prerequisite for firing action potentials[20]. Yet, despite extensive knowledge of the path and strength of corticostriatal communications[6, 17], there has been little understanding of which communications tend to be transmitted concurrently with one another. Put another way, while the literature has elucidated a tremendous amount about coordination within cortex-striatum node-pairs, comparatively little is known about coordination between them.

Here, we computed moment-by-moment (albeit, at a resolution of 720 msec) coactivation magnitudes in cortex-striatum node-pairs (edges) – between which communications are transmitted across well-characterized monosynaptic connections – as a proxy for temporal patterns of communication intensity. We found that there is a tremendous diversity of corticostriatal communication patterns, as >94% of corticostriatal edge-pairs have coactivation patterns with low synchrony (eFC < 0.2). Nonetheless, corticostriatal node-pairs can be robustly and reproducibly clustered into a small set of communities with similar communication patterns. We made the striking observation that the spatial distribution of these communities with similar frontal communication patterns is not aligned with the spatial distribution of communities that have similar structural and static FC with frontal cortex. Classic maps have long shown that spatial communities in the striatum with similar structural and

static FC with frontal cortex manifest as diagonal bands oriented in a dorsomedial-to-ventrolateral fashion[6, 17]. In contrast, we found that spatial communities in the striatum with similar frontal communication patterns manifest as diagonal bands oriented in a ventromedial-to-dorsolateral fashion – largely orthogonal to the classic bands of structural and static FC. This results in an organization wherein 1) striatal nodes connected to similar areas of cortex may nonetheless communicate with these areas at different times and 2) striatal nodes connected to different areas of cortex may nonetheless communicate with these areas at similar times. This spatiotemporal "blending" may serve to both increase the repertoire of striatal responses to frontal input within functional domains and facilitate coordination across functional domains in the temporal dimension. This type of "blended" circuit organization, wherein gradients of distinct modalities are oriented orthogonally to one another to create a matrix of diverse computational units, has been observed in the visual cortex[40]. Here, orientation columns are organized orthogonally to ocular dominance columns, with different color "blobs" embedded throughout the matrix, to create distinct functional units to process different combinations of orientation, eye and color input[41]. Moreover, this matrix of computational units is highly plastic, both in the context of development and in response to changes in visual input[42]. This exemplar suggests that the spatiotemporal blending observed here in the striatum may establish a previously unrecognized matrix of computational units that warrants future examination in the context of behavior and development.

How might striatal nodes that receive similarly timed communications from similar frontal areas nonetheless have different patterns of coactivation with these frontal areas? We hypothesized that other striatal afferents known to modulate or "gate" striatal responsivity to

frontal cortical input might play a role in this phenomenon. This hypothesis was based on several neurobiological observations. First, within the striatum, MSNs receive an intricate set of modulatory input both from other MSNs via axon collaterals and from a diverse set of striatal interneurons [32-34]. It has been posited that lateral inhibition between MSNs is foundational in regulating MSN excitability to frontal input and shaping behaviorally relevant ensembles of MSNs[34]. The striatum also receives afferents from the bilateral dopaminergic midbrain and thalamus that are known to modulate MSN excitability to frontal cortical input[35, 36]. For instance, thalamic glutamatergic input to striatal cholinergic interneurons is thought to gate the influence of cortical input on striatal MSNs[36], and dopaminergic projections from the substantia nigra and ventral tegmental area are known to directly modulate MSN excitability via interactions with MSN D1 and D2 receptors[35]. Thus, theoretically, if striatal MSNs with similar connectivity profiles with frontal cortex have different profiles of intra-striatal, midbrain-striatal and thalamo-striatal connectivity, these MSNs could have different magnitudes of responsivity to the same frontal input at a given moment in time.

We provide evidence of such a model in our data. The spatial distribution of striatal communities with similar intra-striatal, midbrain-striatal, and thalamo-striatal connectivity profiles differed decidedly from the spatial distribution of striatal communities with similar frontal cortical connectivity profiles. Yet, striatal communities with similar intra-striatal connectivity profiles in particular aligned strongly with striatal communities that have similar frontal cortical coactivation patterns. Collectively, the observations that 1) striatal nodes with similar frontal cortical connectivity profiles can have distinct modulatory input profiles, and that 2) the spatial distributions of striatal communities with similar modulatory input profiles and

similar frontal coactivation patterns were highly aligned, strongly suggests the role of these modulatory inputs in shaping the temporal organization of corticostriatal communications. It should be noted that our examination of these processes is limited by the temporal (720 msec) and spatial (2 mm^3) resolution of fMRI. Functional units of both time and space occur at smaller scales in the striatum[43], and thus follow-up work using electrophysiological techniques is warranted.

Overall, we provide evidence for a systems-level temporal organization of corticostriatal circuitry. Findings and methods provide a framework for using fMRI to investigate how different corticostriatal connections coordinate – via temporal synchrony of their communications – to produce complex behaviors and how these may be altered in various neuropsychiatric diseases.

METHODS

Discovery dataset analyses were performed on rsfMRI data from a cohort of 77 unrelated adult subjects (age: 29.09 ± 3.86; 36.4% male; all right-handed) from the Human Connectome Project (HCP) dataset[30] curated by Chen and colleagues [31] to meet the following stringent standards for low head-motion during scanning: (1) range of head motion in any translational direction less than 1 mm and (2) average scan-to-scan head motion less than 0.2 mm. An age-, gender- and handedness-matched n=77 replication sample (age: 29.08 ± 3.62; 33.8% male; all right-handed) was also drawn from the HCP dataset. Sample matching was performed using nearest neighbor matching via the R program MatchIt (https://cran.r-project.org/web/packages/MatchIt/MatchIt.pdf). Briefly, the program computed a distance between each discovery sample subject and the remaining HCP subjects, and, one-by-one, selected a match for each discovery sample subject. The HCP study was approved by the Washington University Institutional Review Board and informed consent was obtained from all subjects.

fMRI Data Acquisition

HCP neuroimaging data were acquired with a standard 32-channel head coil on a Siemens 3T Skyra modified to achieve a maximum gradient strength of 100 mT/m [30, 44, 45]. Gradient-echo EPI images were acquired with the following parameters: TR = 720 ms, TE = 33.1 ms, flip angle = 52º, FOV = 280 × 180 mm, Matrix = 140 × 90, Echo spacing = 0.58 ms, BW = 2,290 Hz/Px. Slice thickness was set to 2.0 mm, 72 slices, 2.0 mm isotropic voxels, with a multiband acceleration factor of 8. Resting state data used in the present analyses were

acquired from runs of approximately 14.4 min each (REST1). Participants were instructed to lie still with their eyes open and fixated on a bright crosshair on a dark background.

Preprocessing

We began with HCP minimally preprocessed resting-state data [46]. Briefly, this preprocessing pipeline removes spatial distortions, realigns volumes to compensate for subject motion, registers the echo planar functional data to the structural data, reduces the bias field, normalizes the 4D image to a global mean, and masks the data with a final FreeSurfer-generated brain mask [46] We performed further preprocessing steps on each subject's resting-state data including spatial blurring with a 6-mm full-width half-maximum Gaussian kernel and temporal filtering (0.01<f <0.1 Hz). To further minimize effects of subject head-motion, volumes were censored for framewise motion displacement (i.e., volume to volume movement) >0.5 mm [47, 48]. Finally, the time series of each voxel was confound regressed in a GLM with 17 regressors of no interest: six motion parameters (three translations and three rotations) obtained from the rigid-body alignment of EPI volumes and their six temporal derivatives; the mean time series extracted from white matter; the mean times series extracted from CSF; and a second-order polynomial to model baseline signal and slow drift.

To extract the frontal cortical and striatal timeseries of interest, we performed the following steps. First, we parcellated each hemisphere of the frontal cortex into 15 regions of interest (ROIs) using the Harvard-Oxford atlas (http://www.fmrib.ox.ac.uk/fsl/): supplementary motor cortex, superior frontal gyrus, subcallosal cortex, precentral gyrus, paracingulate gyrus, middle frontal gyrus, insular cortex, inferior frontal gyrus pars opercularis, inferior frontal gyrus pars triangularis, frontal pole, frontal orbital cortex, frontal operculum cortex, frontal medial

cortex, central opercular cortex, and anterior cingulate cortex. For each subject, a mean timeseries was computed from the voxels comprising each of the 30 ROIs. Sample-specific right and left striatum masks were created by averaging the union of the caudate, putamen, and nucleus accumbens FreeSurfer parcellations of each subject. This resulted in right and left striatum masks of 1710 and 1712 voxels, respectively; a timeseries was extracted from each voxel. As such, each subject had 1710 right striatal timeseries, 1712 left striatal timeseries, and 30 frontal cortical timeseries. Each of these timeseries was Z-scored. Since we sought to investigate corticostriatal connections and not striatal-striatal connections, analyses were performed separately for the right and left striatum.

Analytic Strategy

Building the Frontostriatal eFC Matrix

To compute corticostriatal edge time series (eTS) and edge functional connectivity (eFC) matrices[27] for each subject, we performed the following steps (see **Figure 1**). For each of the 1710*30=51,300 unique cortical node-striatal node pairs (edges) in the right striatum, we computed the element-wise product of the pair's Z-scored timeseries. The resulting 51,300 eTSs each encoded the magnitude by which activity of the two nodes comprising the edge was synchronized at each moment in time (i.e., at each TR). Increasingly positive values in the eTS represent moments where activity in the two nodes is more synchronized (i.e., where activity is either high or low at both nodes). In contrast, increasingly negative values in the eTS represent moments where activity in the two nodes is less synchronized (i.e., where activity at one node is high while activity in the other node is low). Lastly, the scalar product of each pair of eTSs was taken to compute a 51,300 x 51,300 eFC matrix. Each value in the eFC matrix represents the

correlation between the synchrony magnitudes of two eTSs across time. This provides an index of how similar the temporal pattern of nodal activity synchrony is for two distinct edges. The eFC matrix of each subject was averaged together to establish a group mean eFC matrix, upon which subsequent analyses of interest were performed. An analogous process was undertaken for the left striatum.

Analyzing the eFC Matrix

To cluster edges with similar eTSs into "coactivation synchrony communities", we used a standard *k*-means algorithm with squared Euclidean distance and 1,000 iterations at each value of *k*=2 through *k*=10. To quantify the diversity of each striatal voxel's coactivation synchrony community profile, we computed each profile's entropy, which indexes the uniformity of its distribution of values:

$$H = -\sum_{i=1}^{30} c_i \log_2(c_i)$$

where c_i is the community number the voxel's *i*-th edge[38]. For each voxel we divided this measure by $\log_2 30$ to normalize it and bind it to the interval [0,1][49]. Higher values of entropy indicate voxels whose edges belong to many different communities. Conversely, lower values of entropy represent voxels whose edges belong primarily to the same community.

Defining Edge-Pair Types

To conduct descriptive analyses of the properties of coactivation synchrony across different kinds of corticostriatal connections, we categorized edge-pairs into five "types" (**Supplementary Figure 1**). To define "spatially separated" striatal nodes, we parcellated the striatum into six non-overlapping sub-territories: rostral and caudal caudate, rostral and caudal

putamen, and rostral and caudal nucleus accumbens. The Oxford-GSK-Imanova Structural–Anatomical Striatal Atlas[50] (https://identifiers.org/neurovault.image:406338) was used to guide delineation of caudate, putamen and nucleus accumbens; the anterior commissure was used as an anatomical landmark to delineate rostral versus caudal subdivisions for the caudate and putamen; subdivisions of the nucleus accumbens were determined using the first and second half of coronal slices where the structure appeared. Two striatal nodes situated in two different sub-territories were considered to be "spatially separated"; pairs of striatal nodes where one was located on or adjacent to the border of two sub-territories were not considered as spatially separated. Edges formed between cortical nodes and adjacent striatal nodes were not considered in this "types" framework, given the highly correlated time series of adjacent striatal voxels.

Examining Intra-Striatal, Fronto-Striatal, Midbrain-Striatal, and Thalamo-Striatal Static Functional Connectivity

The correlation between the BOLD timeseries of each striatal voxel and the BOLD timeseries of each of the following were computed: 1) all remaining voxels in the striatum, 2) the 30 frontal cortical ROIs, 3) all voxels in the bilateral midbrain, and 4) all voxels in the bilateral thalamus. Voxel-wise time-series from the midbrain were extracted from masks of the bilateral[51] substantia nigra and ventral tegmental area as defined by Murty et al [52, 53] (https://neurovault.org/images/46839/). Voxel-wise time-series from the bilateral thalamus were extracted from the mask defined by Krauth et al [54, 55] (https://neurovault.org/images/111302/). Thus, each striatal voxel was assigned four independent static connectivity profiles – one with each of the four structures (striatum, frontal

cortex, midbrain, and thalamus). K-means clustering was performed separately for striatal connectivity profiles with each of the four structures, to determine the distinct spatial distribution of striatal connectivity profiles with each structure.

DATA AVAILABILITY

All imaging data come from the Human Connectome Project's publicly available, open access repository at https://db.humanconnectome.org/app/template/Login.vm, which can be accessed after signing a data use agreement.

CODE AVAILABILITY

Code to apply "temporal unwrapping"/edge functional connectivity and its related derivatives to corticostriatal circuits or other circuits/networks of interest has been made available at https://github.com/ckorponay/Temporal_Organization_of_Communications.

Acknowledgements

Data were provided by the Human Connectome Project, WU-Minn Consortium (Principal Investigators: David Van Essen and Kamil Ugurbil; 1U54MH091657) funded by the 16 NIH Institutes and Centers that support the NIH Blueprint for Neuroscience Research, and by the McDonnell Center for Systems Neuroscience at Washington University. Funding for this work was provided by the National Institute on Drug Abuse (1F32DA048580-01A1 to C.K.) and the Intramural Research Program of the National Institute on Drug Abuse (to T.R. and E.A.S.).

References

1. Bressler, S.L. and V. Menon, *Large-scale brain networks in cognition: emerging methods and principles.* Trends in cognitive sciences, 2010. **14**(6): p. 277-290.
2. Damoiseaux, J.S., et al., *Consistent resting-state networks across healthy subjects.* Proceedings of the national academy of sciences, 2006. **103**(37): p. 13848-13853.
3. Power, J.D., et al., *The development of human functional brain networks.* Neuron, 2010. **67**(5): p. 735-748.
4. Di Martino, A., et al., *Functional connectivity of human striatum: a resting state FMRI study.* Cerebral cortex, 2008. **18**(12): p. 2735-2747.
5. Sporns, O., G. Tononi, and R. Kötter, *The human connectome: a structural description of the human brain.* PLoS computational biology, 2005. **1**(4): p. e42.
6. Haber, S.N., *Corticostriatal circuitry.* Dialogues in clinical neuroscience, 2016. **18**(1): p. 7.
7. Pennartz, C.M., et al., *Corticostriatal interactions during learning, memory processing, and decision making.* Journal of Neuroscience, 2009. **29**(41): p. 12831-12838.
8. Morris, L.S., et al., *Fronto-striatal organization: defining functional and microstructural substrates of behavioural flexibility.* cortex, 2016. **74**: p. 118-133.
9. Shepherd, G.M., *Corticostriatal connectivity and its role in disease.* Nature Reviews Neuroscience, 2013. **14**(4): p. 278-291.
10. Kuo, H.-Y. and F.-C. Liu, *Synaptic wiring of corticostriatal circuits in basal ganglia: insights into the pathogenesis of neuropsychiatric disorders.* eneuro, 2019. **6**(3).
11. Selemon, L. and P. Goldman-Rakic, *Longitudinal topography and interdigitation of corticostriatal projections in the rhesus monkey.* Journal of Neuroscience, 1985. **5**(3): p. 776-794.
12. Ferry, A.T., et al., *Prefrontal cortical projections to the striatum in macaque monkeys: evidence for an organization related to prefrontal networks.* Journal of Comparative Neurology, 2000. **425**(3): p. 447-470.
13. Korponay, C., E.Y. Choi, and S.N. Haber, *Corticostriatal Projections of Macaque Area 44.* Cereb Cortex Commun, 2020. **1**(1): p. tgaa079.
14. Alexander, G.E. and M.D. Crutcher, *Functional architecture of basal ganglia circuits: neural substrates of parallel processing.* Trends in neurosciences, 1990. **13**(7): p. 266-271.
15. Choi, E.Y., B.T. Yeo, and R.L. Buckner, *The organization of the human striatum estimated by intrinsic functional connectivity.* Journal of neurophysiology, 2012. **108**(8): p. 2242-2263.
16. Jarbo, K. and T.D. Verstynen, *Converging structural and functional connectivity of orbitofrontal, dorsolateral prefrontal, and posterior parietal cortex in the human striatum.* Journal of Neuroscience, 2015. **35**(9): p. 3865-3878.
17. Gordon, E.M., et al., *Individualized Functional Subnetworks Connect Human Striatum and Frontal Cortex.* Cerebral Cortex, 2021.
18. Choi, E.Y., B.T. Yeo, and R.L. Buckner, *The organization of the human striatum estimated by intrinsic functional connectivity.* J Neurophysiol, 2012. **108**(8): p. 2242-63.

19. Wilson, C.J., *Dendritic morphology, inward rectification, and the functional properties of neostriatal neurons*, in *Single neuron computation*. 1992, Elsevier. p. 141-171.
20. Wilson, C., *The contribution of cortical neurons to the firing pattern of striatal spiny neurons.* Model of Information Processing in Basal Ganglia, 1995. **1**: p. 29-31.
21. Wilson, C.J. and Y. Kawaguchi, *The origins of two-state spontaneous membrane potential fluctuations of neostriatal spiny neurons.* Journal of neuroscience, 1996. **16**(7): p. 2397-2410.
22. Carter, A.G., G.J. Soler-Llavina, and B.L. Sabatini, *Timing and location of synaptic inputs determine modes of subthreshold integration in striatal medium spiny neurons.* Journal of Neuroscience, 2007. **27**(33): p. 8967-8977.
23. Ferry, A.T., et al., *Prefrontal cortical projections to the striatum in macaque monkeys: evidence for an organization related to prefrontal networks.* J Comp Neurol, 2000. **425**(3): p. 447-70.
24. Berke, J.D., et al., *Oscillatory entrainment of striatal neurons in freely moving rats.* Neuron, 2004. **43**(6): p. 883-96.
25. Dzirasa, K., et al., *Noradrenergic control of cortico-striato-thalamic and mesolimbic cross-structural synchrony.* J Neurosci, 2010. **30**(18): p. 6387-97.
26. Koralek, A.C., R.M. Costa, and J.M. Carmena, *Temporally precise cell-specific coherence develops in corticostriatal networks during learning.* Neuron, 2013. **79**(5): p. 865-72.
27. Faskowitz, J., et al., *Edge-centric functional network representations of human cerebral cortex reveal overlapping system-level architecture.* Nature neuroscience, 2020. **23**(12): p. 1644-1654.
28. Chumin, E.J., et al., *Cortico-subcortical interactions in overlapping communities of edge functional connectivity.* NeuroImage, 2022. **250**: p. 118971.
29. Esfahlani, F.Z., et al., *High-amplitude cofluctuations in cortical activity drive functional connectivity.* Proceedings of the National Academy of Sciences, 2020. **117**(45): p. 28393-28401.
30. Van Essen, D.C., et al., *The WU-Minn human connectome project: an overview.* Neuroimage, 2013. **80**: p. 62-79.
31. Chen, T., et al., *Distinct Global Brain Dynamics and Spatiotemporal Organization of the Salience Network.* PLoS Biol, 2016. **14**(6): p. e1002469.
32. Silberberg, G. and J.P. Bolam, *Local and afferent synaptic pathways in the striatal microcircuitry.* Curr Opin Neurobiol, 2015. **33**: p. 182-7.
33. Taverna, S., E. Ilijic, and D.J. Surmeier, *Recurrent collateral connections of striatal medium spiny neurons are disrupted in models of Parkinson's disease.* J Neurosci, 2008. **28**(21): p. 5504-12.
34. Burke, D.A., H.G. Rotstein, and V.A. Alvarez, *Striatal Local Circuitry: A New Framework for Lateral Inhibition.* Neuron, 2017. **96**(2): p. 267-284.
35. Surmeier, D.J., et al., *D1 and D2 dopamine-receptor modulation of striatal glutamatergic signaling in striatal medium spiny neurons.* Trends in neurosciences, 2007. **30**(5): p. 228-235.
36. Ding, J.B., et al., *Thalamic gating of corticostriatal signaling by cholinergic interneurons.* Neuron, 2010. **67**(2): p. 294-307.

37. Korponay, C., E.A. Stein, and T.J. Ross, *Laterality Hotspots in the Striatum.* Cereb Cortex, 2021.
38. Conrad, K., *Probability distributions and maximum entropy.* Entropy, 2004. **6**(452): p. 10.
39. Hebb, D.O., *The organization of behavior: A neuropsychological theory*. 2005: Psychology Press.
40. Hubel, D.H., T.N. Wiesel, and M.P. Stryker, *Anatomical demonstration of orientation columns in macaque monkey.* Journal of Comparative Neurology, 1978. **177**(3): p. 361-379.
41. Bartfeld, E. and A. Grinvald, *Relationships between orientation-preference pinwheels, cytochrome oxidase blobs, and ocular-dominance columns in primate striate cortex.* Proceedings of the National Academy of Sciences, 1992. **89**(24): p. 11905-11909.
42. Hubel, D.H., et al., *Plasticity of ocular dominance columns in monkey striate cortex.* Philosophical Transactions of the Royal Society of London. B, Biological Sciences, 1977. **278**(961): p. 377-409.
43. Shin, J.H., et al., *Spatial organization of functional clusters representing reward and movement information in the striatal direct and indirect pathways.* Proceedings of the National Academy of Sciences, 2020. **117**(43): p. 27004-27015.
44. Glasser, M.F., et al., *The human connectome project's neuroimaging approach.* Nature neuroscience, 2016. **19**(9): p. 1175-1187.
45. Uğurbil, K., et al., *Pushing spatial and temporal resolution for functional and diffusion MRI in the Human Connectome Project.* Neuroimage, 2013. **80**: p. 80-104.
46. Glasser, M.F., et al., *The minimal preprocessing pipelines for the Human Connectome Project.* Neuroimage, 2013. **80**: p. 105-124.
47. Power, J.D., et al., *Spurious but systematic correlations in functional connectivity MRI networks arise from subject motion.* Neuroimage, 2012. **59**(3): p. 2142-54.
48. Yan, C.G., et al., *A comprehensive assessment of regional variation in the impact of head micromovements on functional connectomics.* Neuroimage, 2013. **76**: p. 183-201.
49. Faskowitz, J., et al., *Edge-centric functional network representations of human cerebral cortex reveal overlapping system-level architecture.* Nat Neurosci, 2020. **23**(12): p. 1644-1654.
50. Tziortzi, A.C., et al., *Imaging dopamine receptors in humans with [11C]-(+)-PHNO: dissection of D3 signal and anatomy.* Neuroimage, 2011. **54**(1): p. 264-277.
51. Fox, M.E., et al., *Cross-hemispheric dopamine projections have functional significance.* Proceedings of the National Academy of Sciences, 2016. **113**(25): p. 6985-6990.
52. Murty, V.P., et al., *Resting state networks distinguish human ventral tegmental area from substantia nigra.* Neuroimage, 2014. **100**: p. 580-9.
53. Park, A.T., et al., *Early childhood stress is associated with blunted development of ventral tegmental area functional connectivity.* Developmental cognitive neuroscience, 2021. **47**: p. 100909.
54. Hwang, K., et al., *The human thalamus is an integrative hub for functional brain networks.* Journal of Neuroscience, 2017. **37**(23): p. 5594-5607.
55. Krauth, A., et al., *A mean three-dimensional atlas of the human thalamus: generation from multiple histological data.* Neuroimage, 2010. **49**(3): p. 2053-2062.